REPORT DOCUMENTATION PAGE

Form Approved
OMB No. 0704-0188

1. AGENCY USE ONLY (Leave blank)	2. REPORT DATE	3. REPORT TYPE AND DATES COVERED
		FINAL

4. TITLE AND SUBTITLE

5. FUNDING NUMBERS

61102F
6101/00

6. AUTHOR(S)

Prof Steve Hersee

7. PERFORMING ORGANIZATION NAME(S) AND ADDRESS(ES)

University of New Mexico

8. PERFORMING ORGANIZATION REPORT NUMBER

AFOSR-TR- 95 0148

9. SPONSORING/MONITORING AGENCY NAME(S) AND ADDRESS(ES)

AFOSR/NE
110 Duncan Avenue Suite B115
Bolling AFB DC 20332-0001

10. SPONSORING/MONITORING AGENCY REPORT NUMBER

F49620-92-J-0526

11. SUPPLEMENTARY NOTES

12a. DISTRIBUTION/AVAILABILITY STATEMENT

APPROVED FOR PUBLIC RELEASE: DISTRIBUTION UNLIMITED

12b. DISTRIBUTION CODE

13. ABSTRACT (Maximum 200 words)

SEE FINAL REPORT ABSTRACT

14. SUBJECT TERMS

15. NUMBER OF PAGES

16. PRICE CODE

17. SECURITY CLASSIFICATION OF REPORT	18. SECURITY CLASSIFICATION OF THIS PAGE	19. SECURITY CLASSIFICATION OF ABSTRACT	20. LIMITATION OF ABSTRACT
UNCLASSIFIED	UNCLASSIFIED	UNCLASSIFIED	UNCLASSIFIED

AFOSR-TR- 95 0148

Final Report
AFOSR Contract F49620-92-J-0526

Professor Steve Hersee
Professor Kevin J. Malloy
The Center for High Technology Materials
EECE Building., Room 125
The University of New Mexico
Albuquerque, New Mexico 87131-6081

SUBMITTED TO:
Dr. H. R. Schlossberg
AFOSR/NE
110 Duncan
Bolling AFB, DC 20332-6448
(202) 767-4906

INTRODUCTION:

The major accomplishments under this contract were the development of a quantum well intersubband photoconductive (QUIP) IR detector growth and fabrication process and characterization of GaN-based ultraviolet detectors.

QUIP IR Detectors:

GROWTH: LWIR Detector Epitaxial Structure (first growth)

CHTM's design of the first epitaxial device structure grown for this program (Fig. 1), was based on LWIR structures published in the public domain and used by leading groups and in this field (AT&T and Aerospace Corporation). This was in keeping with the first-phase goal of this effort, which was to establish a baseline reference device that repeated the "state of the art", rather than to "re-invent the wheel." (Minor differences between CHTM's and other designs were implemented for consistency with our process technology.)

The first growth part of the campaign involved growing calibration structures to establish MOCVD process conditions for the following structural parameters:

1. Composition of the $Al_{0.25}Ga_{0.75}As$ quantum well barrier layers.

The quantum well barrier composition was measured using photoluminescence (PL), where the peak PL wavelength was directly translated to a composition value.

2. Thickness of the 40A GaAs quantum well regions.

The thickness of the GaAs quantum well region (nominally 40A) was checked by two independent techniques. The peak PL wavelength was measured at 813.5 nm. By comparing this wavelength to that for bulk GaAs, an estimate of quantum well thickness between 45A and 48A was obtained. Cross-sectional TEM was also performed on the quantum well region, and the natural difference in atomic contrast allowed the quantum well width to be directly measured with an estimated accuracy of ~ 2%. This measurement fixed the quantum well thickness at between 43A and 45A and also yielded a barrier thickness value (nominally 500A) of between 518A and 523A. It was decided to use these calibrations for the first full structure, even though they indicated a slightly thicker quantum well than intended.

3. Quantum well doping level of 10^{18} cm^{-3}.

The doping level was measured using thick (1 to 2 μm) calibration layers that were characterized by C(V) profiling using a commercial "Polaron" profiler.

Having calibrated the MOCVD process the full structure (figure 1) was grown. N-type doping of the contact layers and the quantum wells in this structure, was achieved using Te, which was chosen for its low diffusion coefficient in GaAs and related materials. As a further precaution to avoid doping of the $Al_{0.25}$ $Ga_{0.75}$ As quantum-well barrier layers, only the center 20A of the 40 A quantum wells was doped. The growth of each quantum well therefore proceeded as follows:

1. 10A undoped GaAs
2. 20A Te-doped GaAs at an equivalent bulk doping concentration of $2x10^{18}$ cm^{-3}.
3. 10A undoped GaAs

4. 20 second growth stop (substrate held at temperature under AsH3 flow but with no group III source flow.)

This concept of "center" doping was use previously in the LWIR structure grown by the Aerospace Corporation.

Photoluminescence and cross-sectional TEM measurements were also performed on the full LWIR detector structure and indicated no significant differences between the calibration and full device structural parameters.

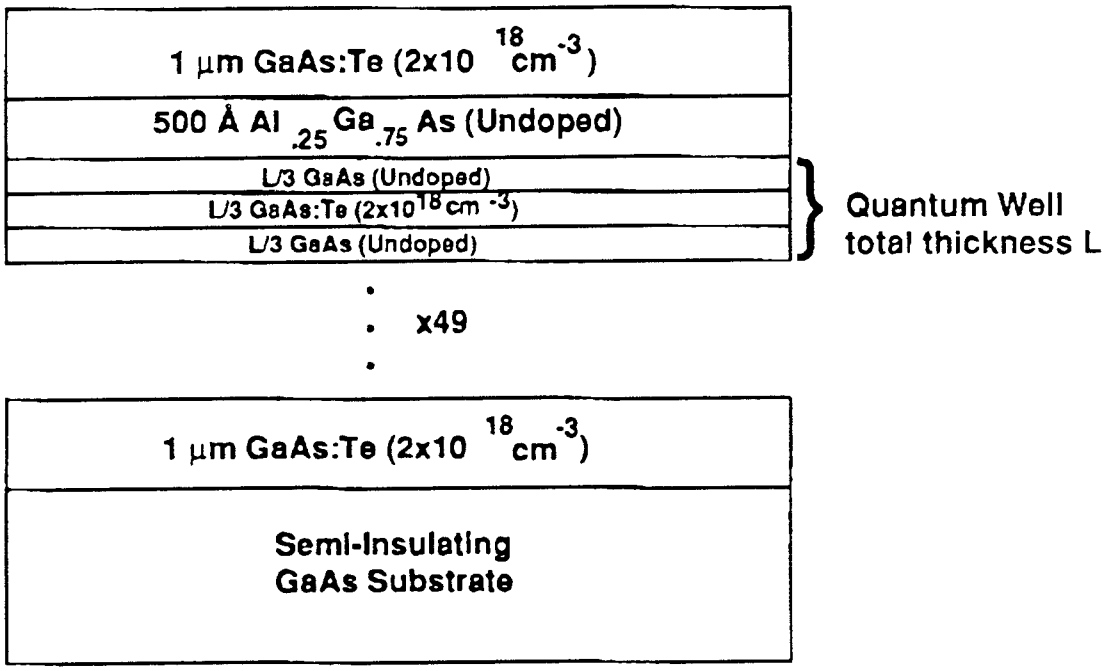

Figure 1. The structure grown by MOCVD in this study.

By dividing up the quantum well into thirds, dopant diffusion and reactor memory effects are minimized. As of this report date, the wafers have been grown, but not yet fabricated. The wafers will be fabricated according to the process described in the next section.

PROCESSING:

A complete fabrication process was developed for the QUIP detectors, taking the as-grown wafers all the way to 68-pin bonded packages. The process schedule sheet is detailed in Appendix II.. When semiinsulating substrates are used, backside illumination can be used and a thin gold film used to cover the top of the mesa. These sample were mounted in a 68-pin chip carrier with a center hole with cryogenic varnish and bonded. For doped substrates, only top illumination can be used, making the hole in the package unneccessary.

Details of the mask design are provided in Appendix II. The mask contains 2x2 arrays of devices with three different mesa sizes: 200 μm, 166 μm and 133 μm on edge. A previous mask set using 200 μm and 100 μm mesas with different ohmic metallization patterns was also tried. Implementation of two dimensional gratings by double exposure of the grating mask was also accomplished, but as we have yet to measure a successful detector, results are not available.

CHARACTERIZATION:

Characterization efforts involved three separate tasks. The first involved TEM and photoluminsecence calibration of the as-grown wafers. The second task, on characterization of the grating profile, was initiated but not completed during this effort. Figure 2 shows SEM micrographs of the grating profile observed in the first two growth runs of this program. The grating walls are seen to be sloped at an angle of approximately 54°, consistent with the anisotropic behavior of the wet chemical etchant used. An analysis of the effect of grating periodicity on diffraction eficiency is shown in Fig. 3. A finite difference, Maxwell equation solver, developed by Professor S. Naqvi and modified for use on QUIP detectors was used for this calculation. We first note that the TE polarization case (electric field along the direction of the grating lines) will NOT

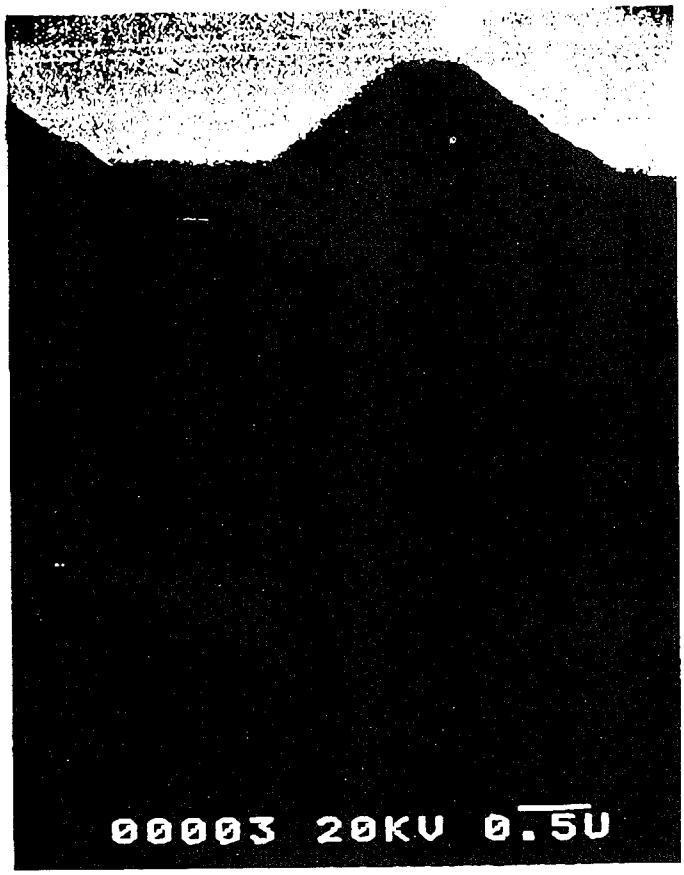

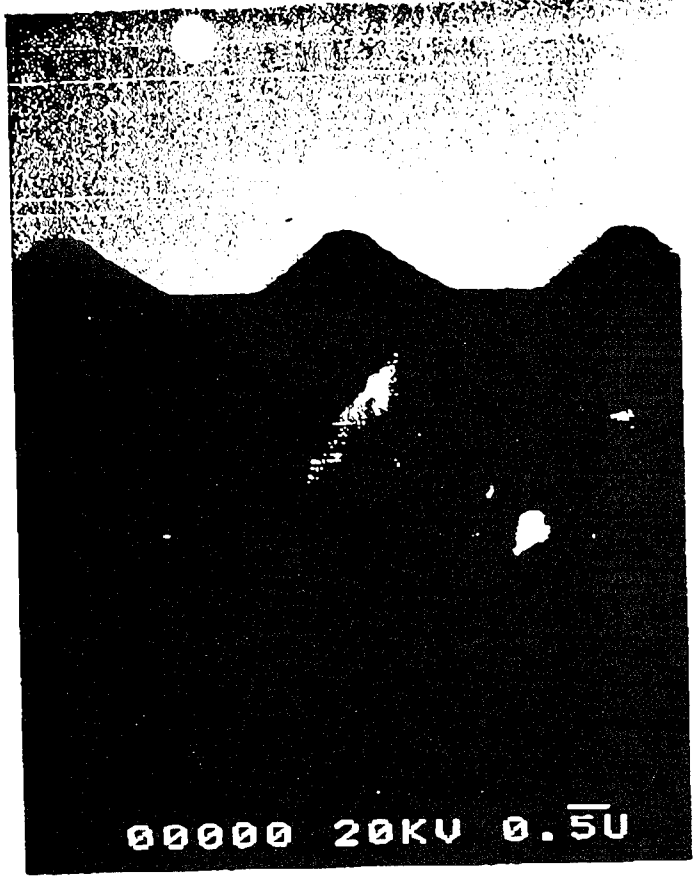

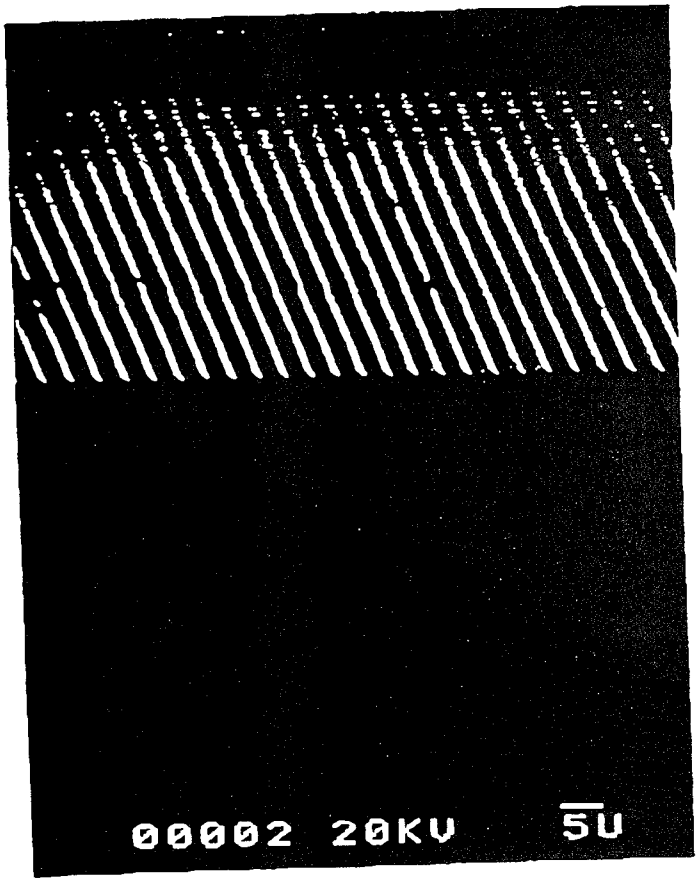

Figure 2. SEM photographs of the grating profile showing the lattice-plane dependence of the anisotropic wet chemical etch rate. The angle made by the grating sidewalls with the surface normal is approximately 54°.

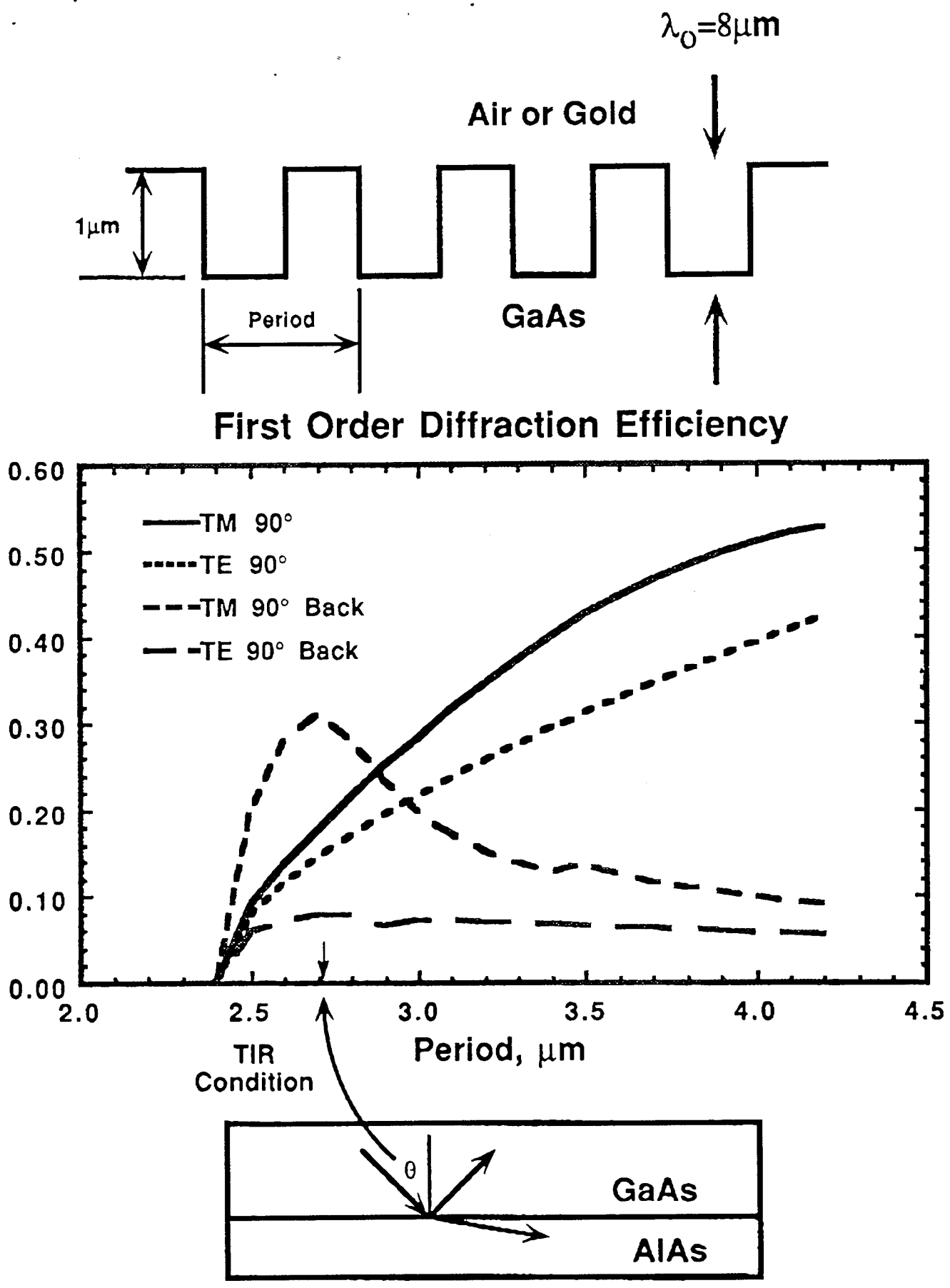

Figure 3. A calculation of the diffraction efficiency of 8 μm radiation incident from the top and bottom of a 1 μm deep GaAs grating as a function of the grating period for a square profile grating. Note that the TE polarization (electric field along the grating lines) does not couple to the QUIP detector. The period where total internal reflection would occur with respect to an underlying AlAs layer corresponds closely to a maximum in the backside illuminated TM diffraction efficiency

result in absorption in the quantum well intersubband transition. On the TM case will give a component of the electric field in the diffracted beam that is along the growth direction and giving intersubband absorption. Furthermore, the first order diffraction efficiency decreases to zero as the condition for a 90° turn in the 8 μm incident radiation is reached. This makes sense as at this periodicity, the first order diffraction becomes evanescent. Unfortunately, experimental concerns prevented us from continuing this modelling effort once the program was developed. Further modeling is needed to include the effects of the evanescent orders on overall efficiency, to understand the effect of actual profiles, and to extend the modeling to two dimensional and random gratings.

The third characterization effort involved the preliminary electrical characterization performed at the University of New Mexico. Figure 4 shows the IV curves at 80K for two different 200 μm-on-edge mesas. In both cases, 100 nA leakage current is exceeded between 2 and 4 V bias in each direction.

GaN DETECTOR DEVELOPMENT:

The family of group III nitrides (AlN, GaN and InN) represents a direct band gap materials system capable of covering the red to the deep UV (Fig 5). The Air Force's interest is UV detectors and as such concentrates on the GaN/AlN materials system. Usually, a sapphire (Al_2O_3) substrate is used with two different Al-O bond lengths (1.85Å and 1.97Å). However, while the lattice of both GaN and sapphire are of hexagonal symmetry, the lattice structure is very different. Thus, the nature of the GaN/Al_2O_3 interface was of great interest to us and of potentially great import for device performance. The results of our investigations are reported in Appendix III, which will appear in a future volume

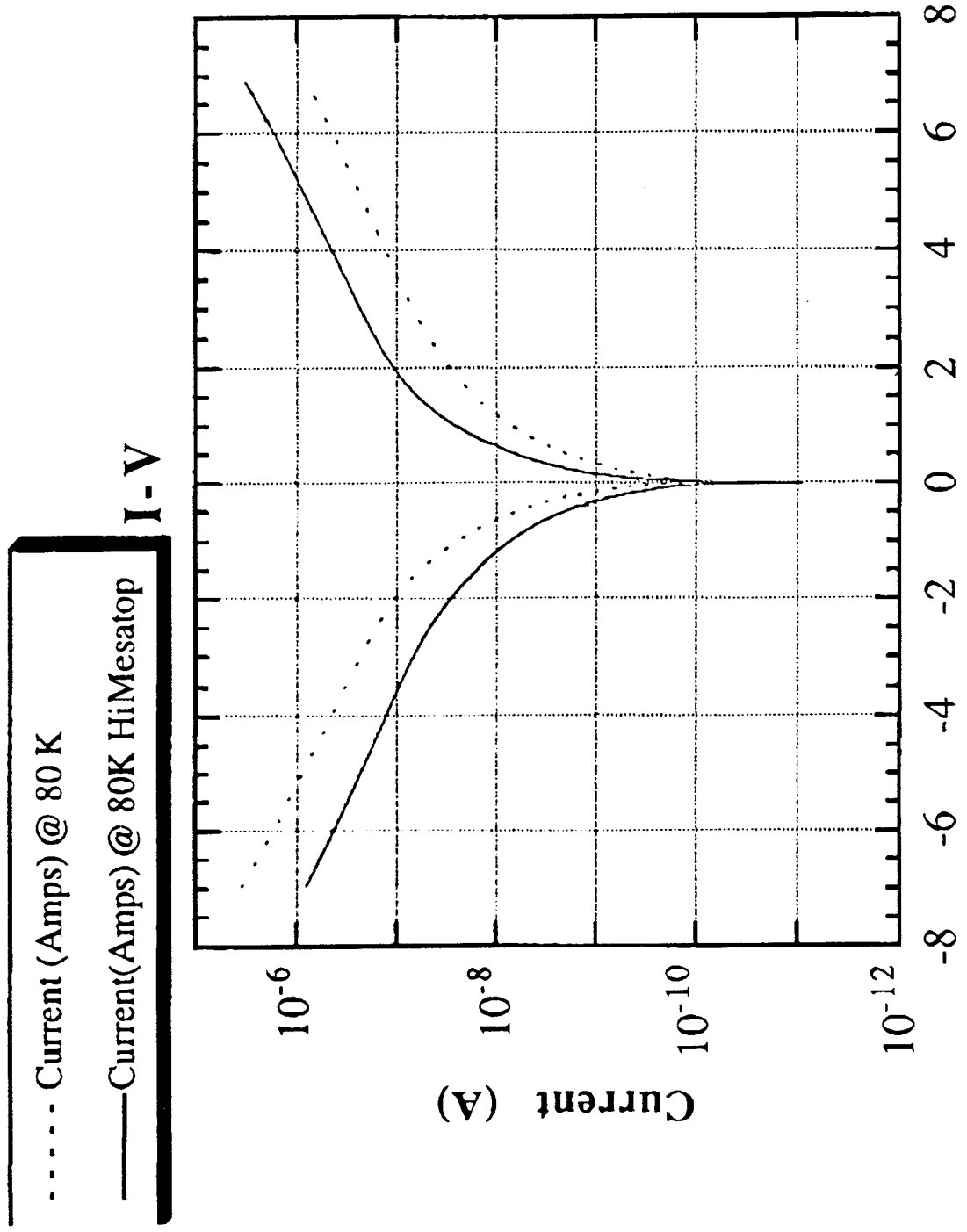

Figure 4. Low temperature (80 K) IV curves for two different 200 μm detectors in the dark. The dark current compares favorably with reported results for $Al_{0.25}Ga_{0.75}As$ barriers.

of the MRS symposia proceedings. Our conclusion was two-fold: 200 Å of AlN serves as an effective buffer layer between GaN and Al_2O_3, and that approximately 10^8 to 10^{10} dislocations per cm^2 exist at the interface. Further research should indicate whether this extremely large concentration effects device performance.

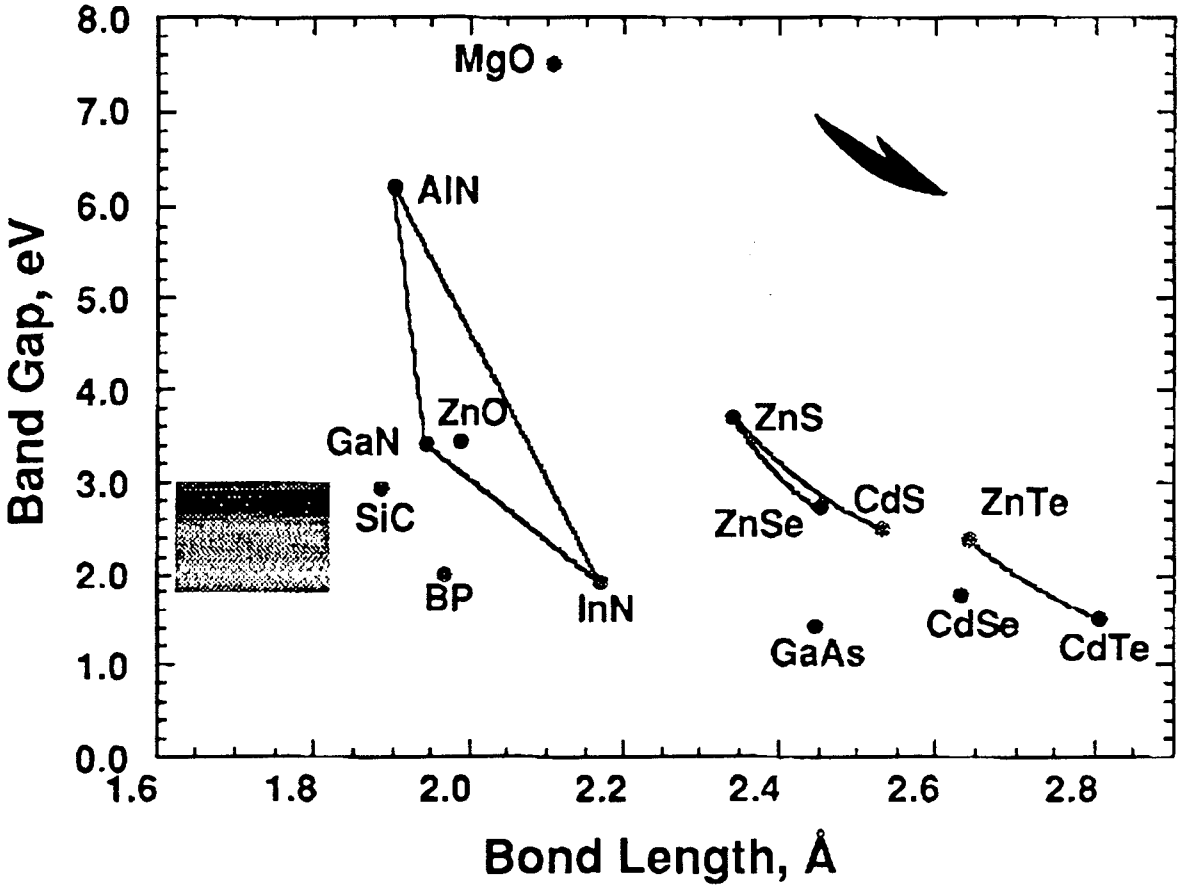

CONCLUSION

Growth, fabrication and characterization procedures have been developed and implemented for quantum well intersubband photoconductive detectors grown by MOCVD. Of the first three detector growth runs, two showed only the tail of a high energy photoresponse while the third sample became debonded under testing. Three new structure have been grown on a new reactor that include the lessons learned from the earlier runs. The fabrication process has been improved